



Uncertainty-Aware Hypergraph Representation Learning for Neurodegenerative Disease Detection

Manman Yuan^{a,b}, Can Yin^{a,b}, Junlin Li^c, Jun Hu^d, Huijia Li^e ^{*}, Matjaž Perc^{f,g,h,i} ^{*}

^a School of Computer Science, Inner Mongolia University, Hohhot, 010021, China

^b National & Local Joint Engineering Research Center of Intelligent Information Processing Technology for Mongolian, Hohhot, 010021, China

^c Department of Imaging Medicine, Inner Mongolia Autonomous Region People's Hospital, Hohhot, 010010, China

^d School of Economics and Management, Inner Mongolia University, Hohhot, 010021, China

^e School of Statistics and Data Science, Nankai University, Tianjing, 300071, Slovenia

^f Faculty of Natural Sciences and Mathematics, University of Maribor, Koroska cesta 160, Maribor, 2000, Slovenia

^g Community Healthcare Center Dr. Adolf Drolc Maribor, Ulica talcev 9, Maribor, 2000, Slovenia

^h Department of Physics, Kyung Hee University, 26 Kyungheedaero, Dongdaemun-gu, Seoul, 02447, Republic of Korea

ⁱ University College, Korea University, 145 Anam-ro, Seongbuk-gu, Seoul, 02841, Republic of Korea

ARTICLE INFO

Dataset link: <https://adni.loni.usc.edu>, <https://www.ppmmi-info.org>

Keywords:

Brain network analysis
Hypergraph Representation Learning
Fuzzy theory
Contrastive learning
Uncertainty modeling
Neurodegenerative disease

ABSTRACT

Hypergraph-based representations provide a systematic way to model higher-order interactions among multiple brain regions, which is important for detecting neurodegenerative diseases. However, existing hypergraph learning methods for brain network analysis face two major challenges. First, conventional binarization of functional connectivity neglects intrinsic uncertainty induced by progressive and heterogeneous pathological processes, which can bias network construction. Second, under the limited neuroimaging data, generic contrastive augmentation strategies introduce biologically implausible perturbations, hindering effective representation learning. We propose an Uncertainty-aware Hypergraph Representation Learning framework (UH-FRL) for neurodegenerative disease detection. We first develop an Uncertainty Relationship Construction (URC) module to infer functional connectivity states under uncertainty by leveraging fuzzy set theory and fuzzy inference. To mitigate data scarcity, we introduce a fuzzy contrastive strategy that generates semantically consistent augmented samples guided by the inferred fuzzy connectivity, reducing unrealistic distortions. We further design a Fuzzy Hypergraph Encoder (FHE) that aggregates uncertainty-aware information from hyperedges and node features through fuzzy rule-based modeling and hypergraph message passing, enabling the learning of robust and discriminative representations of brain network organization patterns. We evaluate UH-FRL on two public datasets and one private clinical dataset. The results show that UH-FRL consistently outperforms state-of-the-art methods, demonstrating strong effectiveness and robustness for neurodegenerative disease detection. The code of implementation is available at: <https://github.com/yincan-y/UH-FRL/tree/master>.

1. Introduction

Neurodegenerative diseases, such as Alzheimer's disease (AD) and Parkinson's disease (PD), are significant and growing public health challenges globally [1–3]. Pathologically, these disorders are pathologically characterized by progressive neuronal

* Corresponding author: Matjaž Perc, Huijia Li

E-mail addresses: hjli@nankai.edu.cn (H. Li), matjaz.perc@gmail.com (M. Perc).

<https://doi.org/10.1016/j.chaos.2026.118154>

Received 23 January 2026; Received in revised form 20 February 2026; Accepted 24 February 2026

Available online 3 March 2026

0960-0779/© 2026 Published by Elsevier Ltd.

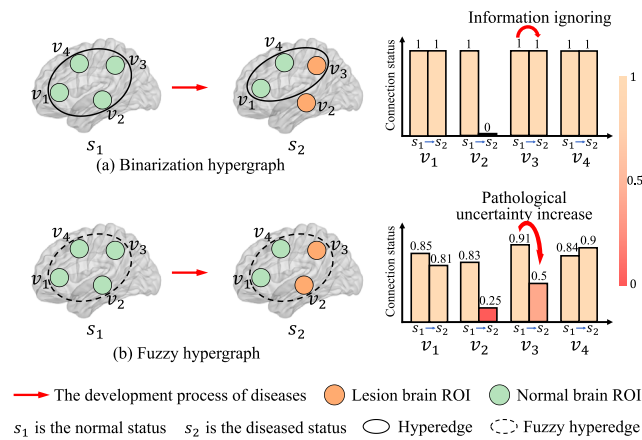


Fig. 1. The evolution of brain network in binarization and fuzzy hypergraphs during the development of the disease. (a) Binarization hypergraph discretizes the functional connectivity state into clear 0/1, ignoring the progressive degradation. (b) Fuzzy hypergraph captures the subtle changes in the connection state, revealing a more detailed pathological mechanism.

degeneration, resulting in irreversible impairments in cognitive, behavioral, and motor functions, thereby placing a considerable burden on both patients' quality of life and social economy [4]. In current clinical practice, disease detection and diagnosis primarily rely on psychiatrists' clinical interviews and behavioral assessments, which are subjective in nature and easily influenced by interrater variability, thereby increasing the risk of misdiagnosis and delayed intervention, especially in the early stages of the disease [5,6]. Therefore, developing objective and data-driven diagnostic frameworks has become essential for improving the accuracy, robustness, and efficiency of early screening for neurodegenerative diseases.

Research has increasingly indicated that neurodegenerative diseases correlate with disease-specific disruptions in functional connectivity patterns among brain regions of interest (ROIs) [7]. Consequently, brain network analysis has emerged as an effective framework for objectively characterizing the underlying pathological mechanisms [8–10]. Among various neuroimaging modalities, functional magnetic resonance imaging (fMRI) has been extensively used for brain network construction, where nodes represent anatomically defined ROIs and edges are determined through using correlation-based measures of blood-oxygen-level-dependent (BOLD) signals between ROI pairs [11]. In this context, the brain network can be naturally modeled as a graph, facilitating systematic analysis of connectivity topology and its perturbations associated with neurodegenerative diseases.

Exploiting the rich information present in fMRI data, deep learning-based brain network analysis methods have gained increasing attention for neurodegenerative disease detection in recent years [12–14]. Specifically, Hypergraph Neural Networks (HGNNs) extend conventional graph models by incorporating hyperedges to encode high-order interactions, such as co-activation patterns and collective information exchange among multiple ROIs. This enables a more precise representation of functional relationships in brain networks [15,16]. Within this framework, hypergraph convolution performs message passing over high-order topological structures, jointly updating feature embeddings across multiple ROIs and learning the discriminative brain network representations. Despite existing HGNNs approaches improve modeling capability for complex connectivity patterns to the pathological mechanisms of neurodegenerative diseases [17,18], they still faces still suffer from several critical limitations.

Primarily, most existing hypergraph-based brain network construction methods rely on similarity metrics and crisp thresholds to binarize functional connectivity, assigning a deterministic membership state to each connection [19,20]. Such methods overlook the uncertainty caused by the progressive nature of disease evolution, as illustrated in Fig. 1. Clinically and biologically, the degradation of functional connectivity in neurodegenerative diseases is not an abrupt event but a continuous and gradual process [21]. Pathological proteins aggregate and propagate along anatomical pathways, preferentially disrupting neurons in network hub regions, resulting in impaired axonal transport and altered inter-regional communication. Over time, this cumulative pathological burden induces cascading failures across multiple spatial scales, ultimately leading to progressive deterioration of functional connectivity. Due to this gradual pathological evolution, it is inherently challenging to define a precise threshold for determining whether a functional connection exists. Additionally, similarity measures-based functional connectivity strengths exhibit continuous distributions [22,23], further blurring the boundary of connectivity states and amplifying uncertainty in network construction. As a result, crisp thresholds and binarization not only introduce subjective bias but also oversimplify the underlying functional brain networks, thereby limiting the ability of downstream models to capture subtle and progressive disease-related alterations.

Second, in the field of medical imaging, the substantial cost of obtaining large-scale, high-quality neuroimaging data and the expert annotation, makes it difficult to construct sufficiently large and reliable brain network datasets, thereby substantially constraining the ability of deep learning models to learn robust and generalizable representations [24–26]. To address this issue of data scarcity, self-supervised contrastive learning has become a promising paradigm, as it allows for the learning of meaningful representations without requiring manual annotations [27,28]. Nevertheless, current contrastive augmentation strategies for brain network analysis predominantly rely on random perturbations of edges, such as randomly removing functional connections between ROIs. This indiscriminates random perturbations may disrupt biologically meaningful connectivity patterns related to

cognitive functions or disease-related alterations, thereby introducing misleading supervisory signals. Consequently, the learned representations are often unstable or semantically incomplete, ultimately limiting the effectiveness of contrastive learning for neurodegenerative disease detection.

To overcome these challenges, this paper proposes an Uncertainty-aware Hypergraph Representation Learning framework (UH-FRL) for neurodegenerative disease detection. First, to explicitly model the uncertainty of functional connectivity states, an Uncertainty Relationship Construction (URC) module is developed, which extracts relationship features among multiple ROIs by multiple similarity metrics, and maps them into two fuzzy sets corresponding to the “existence” and “inexistence” states of functional connections. Through fuzzy inference, the uncertainty of functional connectivity can be effectively captured. Second, to further alleviate data scarcity in brain network analysis, a fuzzy contrastive strategy is introduced that leverages inferred fuzzy connectivity state to construct semantically different positive and negative fuzzy hypergraphs. This approach allows for biologically meaningful data augmentation while preserving critical connectivity patterns associated with cognitive function and disease-related alterations. Finally, we design a Fuzzy Hypergraph Encoder (FHE), which aggregates uncertainty-aware information by the hypergraph message-passing mechanism and encoding node fuzzy representations. The FHE facilitates the learning more discriminative and robust brain network representations for disease detection.

Overall, our contributions can be summarized as follows:

- An Uncertainty Relationship Construction method is proposed to model the uncertainty in functional connectivity caused by the development of the disease.
- we propose a fuzzy contrastive strategy to generate contrastive views which maintains the semantic integrity of biologically meaningful brain network organization.
- A Fuzzy Hypergraph Encoder is developed to learn robust fuzzy representations of brain network from uncertainty-aware hypergraph views.
- Extensive experiments conducted on three datasets reveal that the proposed method outperforms state-of-the-art methods in neurodegenerative disease detection.

2. Related works

2.1. Hypergraph representation learning

Hypergraphs have been increasingly adopted as an effective framework for brain network analysis, modeling the higher-order interactions among multiple ROIs [29–31]. Brain function stems from complex and coordinated co-activation patterns across distributed ROIs, which cannot be adequately characterized by the pairwise relationships assumed in traditional graph models [32]. In hypergraph brain networks, hyperedges connecting multiple ROIs exhibit coherent functional activation patterns, thereby representing high-order interactions within functional modules [31,33]. Such representations more accurately reflect the intrinsic organizational principles underlying human brain function.

Building on this high-order network structure, Hypergraph Neural Networks (HGNNs) have been extensively adopted to learn discriminative brain network representations through message-passing mechanisms with high-order awareness, effective modeling of disease-related connectivity patterns [34–36]. For instance, CcSi-MHAHGEL [37] learns adaptive hyperedge weights to extract multi-atlas-based functional connectivity embeddings. BrainHGNN [38] integrates ROI identity encoding with a random walk-based sampling strategy to preserve both regional characteristics and global network structure. HSIA-GAN [39] captures high-order structural information through node-hyperedge convolution, while STW-MHGNN [12] models spatiotemporal high-order dependencies across brain activity patterns.

Despite these progresses, most existing HGNN-based brain network analysis methods construct hyperedges using binarization connectivity definitions, overlooking the inherent uncertainty in functional connectivity that occurs during disease progression. Consequently, such methods fail to capture subtle and progressive pathological alterations, which limits their sensitivity and generalizability in neurodegenerative disease detection.

2.2. Fuzzy representation learning

Fuzzy theory provides a rigorous mathematical framework for modeling uncertainty by fuzzy sets and fuzzy inference mechanisms [40–42]. In recent years, fuzzy theory has been increasingly introduced into deep learning models to improve uncertainty modeling in networked structures such as graph convolutional networks (GCNs) [43,44]. For example, DFGCNN [45] incorporates fuzzy sets and max operators within fuzzy layers to enhance the representation of uncertainty in node features. FuzzyGCN [46] further models network weights and biases as fuzzy numbers and applies fuzzy graph convolution to explicitly propagate uncertainty.

Numerous studies have investigated the uncertainty modeling in graph structures. DFGCN [47] constructs fuzzy graphs by defining similarity-based fuzzy weights among nodes, integrating both feature distances and spatial relationships. FGNN [48] formulates node relationships as fuzzy membership problems and designs membership functions to quantify the degree of association between nodes. While these methods capture structural uncertainty and modestly improve representational expressiveness, they remain primarily data-driven and do not explicitly account for disease-specific mechanisms, limiting their applicability to neurodegenerative diseases analysis.

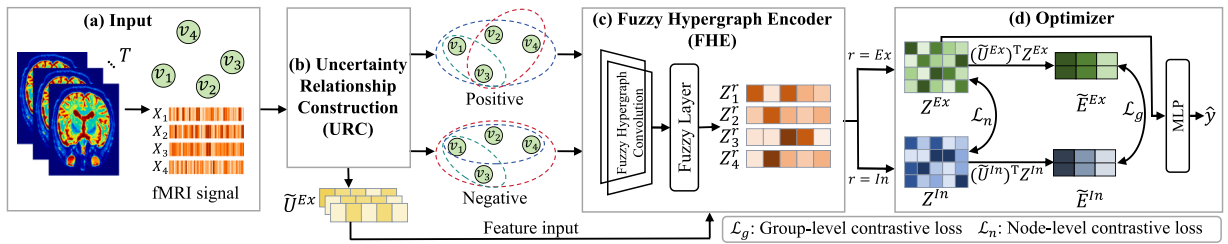


Fig. 2. Framework of UH-FRL. (a) The fMRI signal serves as node feature input for the model. (b) Using fuzzy sets and fuzzy inference to capture uncertainty and constructing positive and negative fuzzy hypergraphs. (c) Aggregating fuzzy information from hyperedges and node features for robust fuzzy representation learning. (d) Achieving model optimization by Group-level and Node-level contrastive loss, and performing the final disease detection.

Beyond graph learning, fuzzy theory has been extensively utilized to address inherent uncertainty and fuzziness present in medical data analysis [49]. For instance, a fuzzy logic-based deep learning framework [50] introduces fuzzy boundaries into medical image analysis for lesion detection, yielding predictions that align more closely with clinical reasoning. Similarly, FGNNs [51] enhance the uncertainty-aware reasoning capability of conventional GNNs through fuzzy logic-based inference mechanisms. A multi-modal teacher–student fusion strategy [52] that leverages Monte Carlo dropout to quantify uncertainty in magnetic resonance brain tumor segmentation for improved robustness, as well as a novel feature selection method [53] that introduces an uncertainty-weighted loss function based on the Dirichlet distribution to model uncertainty across neuroimaging views. However, the integration of fuzzy learning with disease modeling remains limited. In particular, most existing approaches rarely design uncertainty modeling strategies grounded in pathogenesis-driven disease mechanisms, which restricts both their predictive performance and interpretability in biomedical applications.

3. Preliminary

In functional brain networks, the high-order structural relationships with uncertainty are modeled as a fuzzy hypergraph $G = (\mathcal{V}, E, \mathcal{W}, \tilde{U})$, where $\mathcal{V} = \{v_1, v_2, \dots, v_n\}$ denotes the set of nodes corresponding to n ROIs, and $E = \{e_1, e_2, \dots, e_m\}$ represents the set of m fuzzy hyperedges. Each hyperedge $e_i = \{v_{i1}, v_{i2}, \dots, v_{ij}\}$, where $i \in \{1, 2, \dots, m\}$ and $j \in \{1, 2, \dots, n\}$. Each hyperedge corresponds to a potential high-order functional interaction among a subset of ROIs. $\mathcal{W} = \text{diag}(\{w(e_i)\}_{i=1}^m) \in \mathbb{R}^{m \times m}$ is a diagonal matrix, where each diagonal element $w(e_i)$ corresponds to the weight of a fuzzy hyperedge. The uncertainty of node–hyperedge associations is encoded by the fuzzy incidence matrix $\tilde{U} \in \mathbb{R}^{n \times m}$, with element $\tilde{U}_{ij} \in [0, 1]$ indicating the membership degree that node v_i belongs to hyperedge e_i . From the above definitions, the node degree matrix and the hyperedge degree matrix are established as $D_v = \text{diag}(\{d(v_i)\}_{i=1}^n)$ and $D_e = \text{diag}(\{\delta(e_i)\}_{i=1}^m)$, where the degree of node v_i is represented as $d(v_i) = \sum_{e_j \in E} w(e_j) \tilde{U}_{ij}$, and the degree of hyperedge e_i is defined as $\delta(e_i) = \sum_{v_j \in \mathcal{V}} \tilde{U}_{ji}$.

4. Method

In this section, we present the proposed UH-FRL framework for uncertainty-aware brain network representation learning, which comprises two main components: the Uncertainty Relationship Construction (URC) module and the Fuzzy Hypergraph Encoder (FHE), as depicted in Fig. 2.

4.1. Input

The proposed UH-FRL framework takes preprocessed fMRI data as input. For each subject, the brain is segmented into M ROIs utilizing the Automated Anatomical Labeling (AAL) atlas. Subsequently, the mean BOLD time series is then extracted from each ROI to characterize feature of regional hemodynamic activity, generating a feature matrix $X \in \mathbb{R}^{M \times T}$, with T denotes the number of time points. Each row $X_i \in \mathbb{R}^T$ represents the temporal signal of the i th ROI and serves as the initial node feature for relationship modeling in the URC module.

4.2. Uncertainty Relationship Construction (URC)

As previously analyzed, neurodegenerative processes driven by the accumulation of pathological proteins interfere with axonal transport and progressively propagate across ROIs, leading to a gradual degradation of functional connectivity. This pathomechanism makes the “existence” state of functional connections inherently ambiguous, thereby introducing uncertainty. In light of this, we aim to develop an efficient framework that explicitly models uncertainty in functional connectivity among multiple ROIs by integrating fuzzy theory, as demonstrated in Fig. 3.

Relationship Feature Extraction. Functional connectivity is characterized by biological complexity and heterogeneity, such that single similarity metric cannot fully reflect the interactions among ROIs, hindering the accurate representation of uncertainty

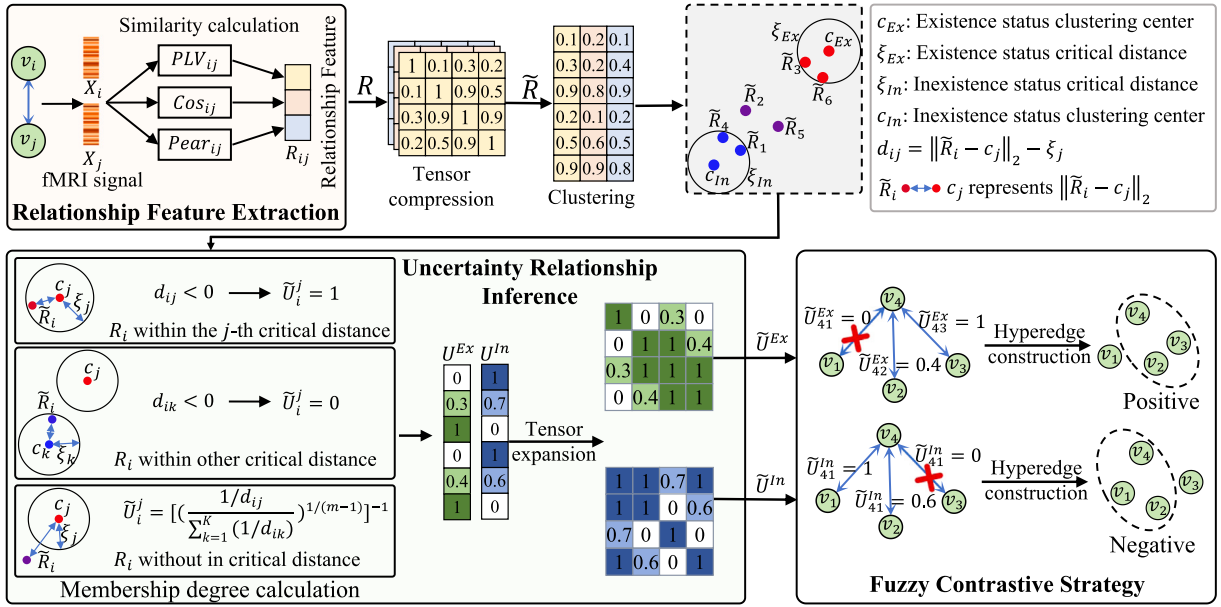


Fig. 3. Detailed introduction of the Uncertainty Relationship Construction module. First, the Relational Feature Extraction submodule extracts relationship features by multiple similarity measures. Then, the Uncertainty Relationship Inference submodule adopts the Fuzzy C-Means algorithm with critical distance to calculate the membership degrees for the ‘existence’ and ‘inexistence’ states fuzzy sets. Based on this, a fuzzy contrast strategy is designed to construct positive and negative fuzzy hypergraph.

in connectivity state. In contrast, multiple complementary similarity metrics construct relationship features enables characterize comprehensive functional interactions, offering a robust data foundation for quantifying uncertainty in functional connectivity.

For each subject, relationship features between a given ROI i and the remaining ROIs are derived based on the fMRI data X to characterize synchronous activation patterns and capture higher-order inter-regional functional interactions. The relationship feature R_{ij} between i th node X_i and j th node X_j is defined as:

$$R_{ij} = [PLV_{ij}, Cos_{ij}, Pear_{ij}], \tag{1}$$

where Cos_{ij} and $Pear_{ij}$ denote the cosine similarity and Pearson correlation, respectively. PLV_{ij} signifies the Phase Locking Value (PLV), which measures phase synchrony between electrophysiological signals and is given by:

$$PLV_{ij} = \frac{1}{T} \left| \sum_{l=1}^T e^{\tau(\Delta\phi_{ij}(t_l))} \right|, \tag{2}$$

where $\Delta\phi_{ij} = (\phi_i(l) - \phi_j(l))$ is the instantaneous phase difference between BOLD time series of ROIs i and j at time index l . $\phi_i(l)$ and $\phi_j(l)$ are derived from X_{ii} and X_{jj} through using the Hilbert transform, where $l \in 1, \dots, T$.

The relationship feature $R \in \mathbb{R}^{M \times M \times d_r}$, where d_r denotes the dimensionality of the relationship features, is symmetric with respect to ROI pairs, i.e., $R_{ij} = R_{ji}$. Directly processing all $M \times M$ pairwise relationships results in redundant computation, as each relationship is considered twice. To improve computational efficiency, we compress the tensor into a compact representation $\tilde{R} \in \mathbb{R}^{\frac{M(M-1)}{2} \times d_r}$.

Uncertainty Relationship Inference. Due to progressive pathophysiological deterioration, functional connectivity often exists an fuzzy intermediate state, exhibiting uncertainty between “existence” and “inexistence”. The compressed relationship features \tilde{R} with rich information can capture this intermediate state. To effectively model this uncertainty, we employ fuzzy theory, representing each connection as a degree of membership to the two states, thereby more accurately reflecting the gradual weakening of functional connectivity during disease progression.

Specifically, the Fuzzy C-Means (FCM) algorithm is adopted to model the two connectivity states as two fuzzy sets, establishing the number of clusters $K = 2$. To enhance membership assignment, we introduce a critical distance ξ for each cluster center, such that relationship feature points within this distance attain the maximum membership degree. This improvement overcomes the limitations of accurately capturing functional connectivity states observed in clinical practice and aligns more closely with the

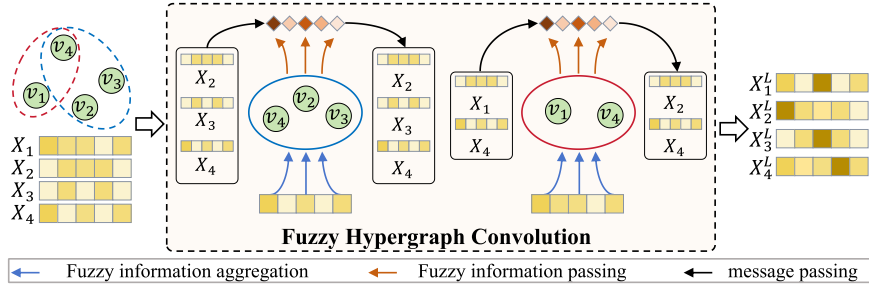


Fig. 4. The Fuzzy Hypergraph Convolution aggregates uncertainty-aware information encoded in the fuzzy association matrix into hyperedges, and passes to node features via hypergraph convolution.

underlying biological mechanisms. Following the study [54], the objective function of the algorithm is redefined as:

$$\begin{aligned} \min_{U^i} J(U) &= \sum_{i=1}^M \sum_{j=1}^K \mu_{ij}^m d_{ij}^2, \\ \text{s.t.} \quad \sum_{j=1}^K \mu_{ij} &= 1, \quad j = 1, 2, \dots, K, \end{aligned} \tag{3}$$

where $d_{ij} = \|\tilde{R}_i - c_j\|_2 - \xi_j$, $\|\tilde{R}_i - c_j\|_2$ denotes the Euclidean distance between i th relationship features $\tilde{R}_i \in \mathbb{R}^{d_r}$ and j th cluster center $c_j \in \mathbb{R}^{d_r}$ with $C = [c_1, c_2, \dots, c_K]$, ξ_j is critical distance of j th cluster center, μ_{ij} denotes the membership degree of the i th relationship features belongs to the j th fuzzy set, m is the fuzzy factor and $U = [\mu_{ij}]^{\frac{M(M-1)}{2} \times K}$ is the membership degree matrix.

To avoid conflicting membership assignments, we impose a constraint on the critical distances ξ_i and ξ_j of any two cluster centers c_i and c_j so that no relationship feature vector simultaneously falls within the critical regions of both centers. Formally, the constraint is expressed as:

$$\xi_i + \xi_j < \|c_i - c_j\|_2. \tag{4}$$

Fuzzy Contrastive Strategy. Due to the limited size of available neuroimaging datasets, learning high-quality brain network representations remains challenging. To address this issue, we introduce a fuzzy contrastive strategy.

In aforementioned algorithm, the relationship feature formed by ROI in conjunction with itself is defined as the cluster center of the “existence” fuzzy set, while the zero vector is defined as the cluster center of the “inexistence” fuzzy set. The membership matrix U^{Ex} corresponding to the “existence” fuzzy set is employed to construct the positive fuzzy hypergraph, whereas the membership matrix U^{In} of the “inexistence” fuzzy set is utilized to construct the negative fuzzy hypergraph. Based on the objective function in Eq. (3) and the constraints in Eq. (4), the updates for the membership matrices are given as follows:

$$U_i^j = \begin{cases} 1, & \text{if } d_{ij} \leq 0, \\ 0, & \text{if } d_{ik} \leq 0, k \neq j, \\ \left[\left(\frac{1/d_{ij}}{\sum_{k=1}^K 1/d_{ik}} \right)^{2/(m-1)} \right]^{-1}, & \text{otherwise,} \end{cases} \tag{5}$$

where $j \in \{Ex, In\}$. After the acquisition of the membership vector $U^{Ex}, U^{In} \in \mathbb{R}^{\frac{M(M-1)}{2}}$, we perform tensor expansion expressed as $\tilde{U}^{Ex}, \tilde{U}^{In} \in \mathbb{R}^{M \times M}$, which respectively serves as the fuzzy incidence matrix of the positive and the negative fuzzy hypergraph.

By modeling the uncertainty related to functional connectivity across different states, we construct positive and negative fuzzy hypergraph brain networks. Fuzzy contrastive strategy not only maintains the intrinsic structure of the brain network by preventing random perturbations of nodes and edges typical in traditional contrastive learning, but also enhances the semantic separation between positive and negative hypergraphs in the representation space. Consequently, our model facilitates the efficient learning subtle alterations in brain network patterns associated with neurodegenerative diseases, even from limited brain network data.

4.3. Fuzzy Hypergraph Encoder (FHE)

Based on the fuzzy incidence matrices U^{Ex}, U^{In} of the positive and negative fuzzy hypergraphs, our goal is to integrate fuzzy information into hypergraph-based brain network representation learning. Therefore, we propose a Fuzzy Hypergraph Encoder embedded into the contrastive learning framework to integrate fuzzy information of hyperedge and node obtaining fuzzy representations. Guided by contrastive learning, the FHE promotes the alignment of representations from positive fuzzy hypergraphs with the intrinsic connectivity patterns of the original brain network, while separating representations of negative fuzzy hypergraphs, thereby establishing a clear structural contrast and enhancing the discriminability of the learned fuzzy representations.

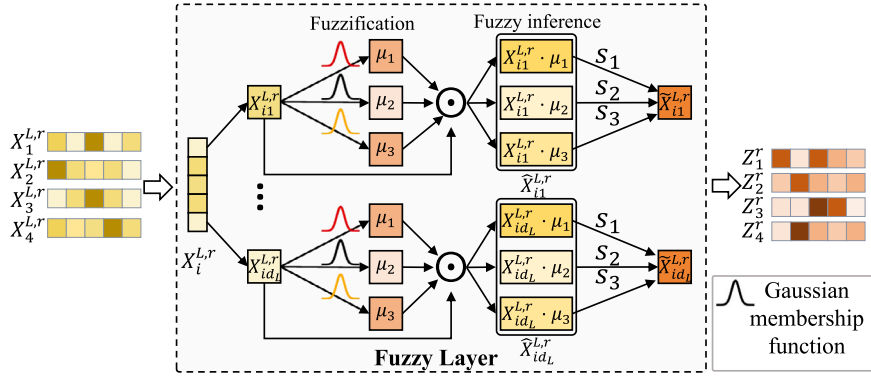


Fig. 5. The Fuzzy Layer adopts fuzzy rules to map input features into fuzzy sets and conducts fuzzy inference to generate fuzzy representations.

To achieve this objective, we first describe the process by which fuzzy information of a hyperedge is aggregated via a hypergraph convolution operation. Subsequently, we explain how the designed fuzzy layers integrate node feature representations in brain ROIs.

Fuzzy Hypergraph Convolution. The high-order aggregation mechanism of hypergraph convolution explicitly encodes fuzzy information in hyperedges and propagates it to node representations, thereby exploiting uncertainty throughout the representation learning process, as illustrated in Fig. 4.

Specifically, the fuzzy incidence matrix of the positive fuzzy hypergraph is first taken as the subject data $X \in \mathbb{R}^{M \times M}$ inputting to the FHE module. Its comprehensive information of brain structure enables the encoder to learning fuzzy representations with enhanced expressiveness and discriminative. Secondly, the weight of each hyperedge e_i through the fuzzy incidence \tilde{U} can be calculated to better extract the fuzzy information on hyperedges as follows:

$$\mathcal{W}_i^{Ex} = \frac{1}{|e_i|} \sum_{v_j \in e_i} \tilde{U}_{ij}^{Ex}, \quad \mathcal{W}_i^{In} = \frac{1}{|e_i|} \sum_{v_j \in e_i} \tilde{U}_{ij}^{In}. \quad (6)$$

Based on the message passing mechanism in HGNNs [18], the l th convolutional layer is expressed as:

$$\begin{aligned} X^{l,Ex} &= \sigma(\text{HGNNconv}(X^{l-1,Ex}, \mathcal{W}^{Ex}, \tilde{U}^{Ex})), \\ X^{l,In} &= \sigma(\text{HGNNconv}(X^{l-1,In}, \mathcal{W}^{In}, \tilde{U}^{In})), \end{aligned} \quad (7)$$

where $X^{l,Ex}, X^{l,In} \in \mathbb{R}^{M \times d_l}$ denotes the output of the l th layer, d_l is output feature dimension. $X^{0,Ex}, X^{0,In} = X$, and σ is the nonlinear activation function. After L convolutional layers, we obtain the encoding representations $X^{L,Ex}, X^{L,In} \in \mathbb{R}^{M \times d_L}$ for the positive and negative fuzzy hypergraphs.

Fuzzy Layer. The process of extracting fuzzy information from node features involves two key operators: fuzzification and fuzzy inference. Fuzzification converts crisp features into fuzzy representations, while fuzzy inference extracts significant fuzzy information, and the details are shown in Fig. 5. Specifically, for node features $X^{L,r}$ with $r \in \{Ex, In\}$, we project them into a fuzzy feature space using Gaussian membership functions, defined as follows:

$$f(X_{ij}^{L,r}) = \exp\left(-\frac{(X_{ij}^{L,r} - t_j)^2}{2\sigma_j^2}\right), \quad j = 1, 2, \dots, d_L, \quad (8)$$

where $X_{ij}^{L,r}$ denotes the j th feature of the i th node, mean t_j and standard deviation σ_j are the trainable parameters. After this transformation, $X_{ij}^{L,r}$ starts to possess fuzziness, indicating the degree belonging to a fuzzy set.

For each node feature, we construct a fuzzy rule base consisting of F rules to model its inherent uncertainty. This mechanism quantifies the degree to which a feature belongs to multiple fuzzy sets and converts the resulting fuzzy memberships into representations that are sensitive to pathology-related variations, yielding more discriminative and robust feature representations. The process is as follows:

$$\left\{ \begin{array}{l} \text{If } x_{ij}^{L,r} \text{ is } A_1^j, \text{ Then } G_1 = \mu_1, \\ \vdots \\ \text{If } x_{ij}^{L,r} \text{ is } A_F^j, \text{ Then } G_F = \mu_F, \end{array} \right. \quad (9)$$

where $A_k^j = f^k(X_{ij}^{L,r})$ represents the Gaussian membership degree function of k th fuzzy set in the j th feature dimension, μ_k denotes the computed membership degree from A_k , and G_k indicates the output of the k th rule.

The outputs of all fuzzy rules form a membership degree vector $\mu = [\mu_1, \dots, \mu_F]^T$, which describes the feature's degree of membership across fuzzy sets. These membership degrees are fused with the original node features through an element-wise product to yield the final fuzzy feature representation, as defined below:

$$\hat{X}_{ij}^{L,r} = X_{ij}^{L,r} \cdot \mu = [X_{ij}^{L,r} \cdot \mu_1, \dots, X_{ij}^{L,r} \cdot \mu_F]^T. \quad (10)$$

Finally, we introduce a learnable rule contribution vector $S = [s_1, \dots, s_F]^T \in \mathbb{R}^F$, which performs a weighted aggregation of the fuzzy feature representations produced by all rules. This enables the model to adaptively emphasize the most informative rules when constructing the final representation, as defined below:

$$\tilde{X}_{ij}^{L,r} = S^T \hat{X}_{ij}^{L,r}. \quad (11)$$

In contrast to max- or min-based fuzzy inference schemes that retain only the dominant rule and discard information from other rules, the proposed method preserves the activation information across all fuzzy rules. Meanwhile, unlike simple mean aggregation, the learnable weighted fusion mitigates over-smoothing effects that dilute distinctive feature representations. Therefore, we obtain the fuzzy representations Z^{Ex} and Z^{In} for the positive and negative hypergraphs, respectively. Z^{Ex} is subsequently fed into a multilayer perceptron (MLP), which outputs the predicted label \hat{y} for graph-level disease classification, as defined below:

$$\hat{y} = MLP(Z^{Ex}). \quad (12)$$

4.4. Optimizer

The overall objective function of the UH-FRL contains three kinds of loss terms as follows:

$$\mathcal{L} = \mathcal{L}_{cls} + \lambda_n \mathcal{L}_n + \lambda_g \mathcal{L}_g, \quad (13)$$

where λ_n and λ_g represent the hyperparameters. The following presents a detailed description of each loss term.

Classification Loss. For each $t \in N$ subject, the predicted label \hat{y}_t and true label y_t are employed to compute the classification loss via the cross-entropy function, defined as follows:

$$\mathcal{L}_{cls} = -\frac{1}{N} \sum_N (y_t \log(\hat{y}_t) + (1 - y_t) \log(1 - \hat{y}_t)). \quad (14)$$

The Node-level Contrastive Loss. To enhance the discriminative power of the learned fuzzy representations and explicitly capture the difference between the ‘‘existence’’ and ‘‘inexistence’’ connectivity states, a node-level contrastive loss is introduced between the positive and negative fuzzy representations, Z^{Ex} and Z^{In} . Following the study [29], the contrastive loss for a positive node pair (v_i, u_i) , is defined as:

$$\ell(v_i, u_i) = -\log \frac{e^{\frac{S(v_i, u_i)}{\rho_n}}}{e^{\frac{S(v_i, u_i)}{\rho_n}} + \sum_{k \neq i} \left[e^{\frac{S(v_i, v_k)}{\rho_n}} + e^{\frac{S(u_i, u_k)}{\rho_n}} \right]}, \quad (15)$$

where ρ_n is a temperature coefficient, $S(\cdot)$ denote the cosine similarity function between two nodes. The objective function for node-level contrast is the average over all positive pairs:

$$\mathcal{L}_n = \frac{1}{2|V|} \sum_{i=1}^{|V|} [\ell(v_i, u_i) + \ell(u_i, v_i)]. \quad (16)$$

The Group-level Contrastive Loss. The group-level contrastive loss aims to distinguish the representations of the same hyperedge across two augmented views from those of other hyperedges. Then, hyperedge features are constructed by using the fuzzy incidence matrix \tilde{U}^{Ex} , \tilde{U}^{In} and the embeddings Z^{Ex} , Z^{In} of the positive and negative hypergraphs, which formulated as follows:

$$\tilde{E}^{Ex} = (\tilde{U}^{Ex})^T Z^{Ex}, \quad \tilde{E}^{In} = (\tilde{U}^{In})^T Z^{In}. \quad (17)$$

The loss function of group-level for each positive hyperedge pair (e_i, h_i) is defined as:

$$\ell(e_i, h_i) = -\log \frac{e^{\frac{S(e_i, h_i)}{\rho_g}}}{e^{\frac{S(e_i, h_i)}{\rho_g}} + \sum_{k \neq i} \left[e^{\frac{S(e_i, e_k)}{\rho_g}} + e^{\frac{S(h_i, h_k)}{\rho_g}} \right]}, \quad (18)$$

where ρ_g is a temperature parameter. The objective function for group-level contrast is defined as:

$$\mathcal{L}_g = \frac{1}{2|E|} \sum_{i=1}^{|E|} [\ell(e_i, h_i) + \ell(h_i, e_i)]. \quad (19)$$

5. Experiments

5.1. Experimental settings

Datasets. We evaluated the UH-FRL method on two public and a private datasets. The Alzheimer’s Disease Neuroimaging Initiative (ADNI) contains 43 Alzheimer’s disease (AD) subjects, 51 mild cognitive impairment (MCI) subjects, and 74 normal controls (NC).

Table 1
Statistics of the datasets in ADNI and PPMI.

Dataset	Group	Number	Group		Age
			Male	Female	
ADNI	NC	74	29	45	74 ± 16
	MCI	51	33	18	72.5 ± 16.5
	AD	43	27	16	71.5 ± 16.5
PPMI	NC	48	31	13	62 ± 10
	PD	98	67	31	64 ± 11
PSCI	NC	28	16	12	76 ± 6.1
	SD	20	15	5	77 ± 5.3

The Parkinson’s Progression Markers Initiative (PPMI) consists of 98 Parkinson’s disease (PD) subjects and 48 NC. The private post-stroke cognitive impairment (PSCI) dataset was collected at the Department of Neuroradiology, Inner Mongolia People’s Hospital, and consists of 20 stroke patients (SD) and 28 NC. The clinical and demographic characteristics are detailed in [Table 1](#).

Processing. To extract BOLD signals from fMRI data, raw functional images were preprocessed using the Data Processing Assistant for Resting-State fMRI (DPARSF) package. Initially, the raw fMRI data were converted into the Neuroimaging Informatics Technology Initiative (NIFTI) format, and the first 10 temporal volumes were removed to achieve signal stabilization. Slice timing correction was then applied, followed by motion correction. Participants with head motion exceeding 2.5 mm translation or 2.5 degrees rotation were excluded to ensure spatial alignment across time points. Subsequently, the functional images were co-registered to T1-weighted structural images, which were split into gray matter, white matter, and cerebrospinal fluid through Statistical Parametric Mapping (SPM). Next, the images were normalized to the Montreal Neurological Institute (MNI) space via Diffeomorphic Anatomical Registration Through Exponentiated Lie Algebra (DARTEL) and smoothed with a 4-mm full-width using a half-maximum Gaussian kernel to reduce inter-subject variability. Finally, bandpass filtering was performed on the functional time series within the range of 0.01–0.1 Hz. After preprocessing, ROIs were defined using the AAL template, and the mean BOLD signal time series for each ROI was extracted as features representing the corresponding brain regions.

Implementation. To ensure experimental fairness, all methods were implemented using the PyTorch framework in a uniform computational environment, which included an NVIDIA GeForce RTX 4090 GPU. The ADNI dataset was evaluated on NC vs. AD and NC vs. MCI two classification tasks. The PPMI and private PSCI datasets were evaluated on NC vs. PD and NC vs. SD classification tasks, respectively. 10-fold cross-validation was applied to all experiments for performance evaluation. The hyperparameters were set as follows: learning rate = 0.001, weight decay = 0.002, number of epochs = 500, dropout rate = 0.5, and a hidden layer with 64 units. Evaluation metrics included accuracy (ACC), sensitivity (SEN), specificity (SPE), area under the curve (AUC), F1-score (F1), and precision (PRE).

Baselines. We compare the proposed UH-FRL method with several baseline approaches to validate its effectiveness. These baselines include graph-based neural networks such as GCNII [55] and CAGNN [56], as well as brain network-based methods like BGAN [57], XG_GNN [58], and GCNH [59]. Additionally, we consider hypergraph-based neural network methods like HGNN [18], WHGCN [17] and TriCL [60], along with hypergraph brain network methods like MHSA [61]. Finally, we evaluate fuzzy deep learning methods like HDFIS [62].

5.2. Comparison with state-of-the-art methods

The results of the comparison with baseline methods are presented in [Tables 2](#) and [3](#), where † indicates the methods augmented with the proposed URC module. The results indicate that our UH-FRL consistently outperforms all baseline methods across the ADNI, PPMI, and PSCI datasets. The baseline methods that incorporate the URC module also exhibit improved performance, providing strong evidence that capturing functional connectivity uncertainty is crucial for accurately characterizing brain networks. This improvement can be attributed to two main factors: (1) Fuzzy Hypergraph Construction employs membership degrees to quantify uncertainty, reflecting progressive degeneration of connection states caused by disease pathology, uncovering subtle alterations in brain network organization associated with disease progression. (2) FHE aggregates Uncertainty from node features and hyperedges through fuzzy incidence matrices and fuzzy rules, refining this information into highly discriminative brain network embeddings that enable more precise disease classification.

5.3. Ablation study and analysis

To evaluate the effectiveness of each module in the UH-FRL, we conducted an ablation study, and the results are detailed in [Table 4](#). The variants are designed as follows:

- **w/o U** replaces the uncertainty relationship construction module with a traditional KNN-based hypergraph construction.
- **w/o FE** removes the aggregation of hyperedge fuzzy information in the fuzzy hypergraph encoder.

Table 2

The classification results of the UH-FRL method and comparison method (%) on ADNI dataset, where G, HG and HFG respectively represent graph, hypergraph and fuzzy hypergraph.

Method	NC vs. AD						NC vs. MCI						
	ACC	SEN	SPE	AUC	F1	PRE	Acc	SEN	SPE	Auc	F1	PRE	
G	GCNII	70.87	33.76	86.91	60.34	64.69	63.71	65.60	78.26	58.48	68.37	61.76	75.01
	CAGNN	72.35	37.5	91.43	64.46	65.93	69.72	77.88	51.00	97.14	74.07	74.52	79.72
	BGAN	75.91	94.07	34.71	64.39	81.73	72.89	68.21	48.81	86.15	67.48	55.09	83.83
	XG_GNN	79.50	48.33	89.25	68.79	53.14	72.83	71.02	50.17	84.52	67.34	54.08	80.00
	GCNH	75.00	50.00	88.57	69.29	70.88	73.72	76.99	70.00	81.79	75.89	73.47	76.08
	HGNN	78.63	42.97	94.57	68.77	52.38	73.33	77.05	53.00	93.88	73.44	61.81	82.91
	WHGCN	81.36	61.43	98.75	80.09	70.74	97.50	81.92	86.50	75.37	80.93	79.08	74.86
	TriCL	76.06	53.67	89.86	71.76	60.11	85.35	72.95	70.86	71.24	71.05	67.22	68.63
	MHSA	75.91	47.90	91.42	69.46	53.24	72.14	73.78	55.00	87.32	71.16	55.31	66.81
	HDFIS	68.78	66.76	70.91	61.94	75.07	81.03	71.78	63.19	67.85	66.33	67.95	56.74
UH-FRL	84.02	76.67	85.47	81.07	77.84	88.33	83.84	65.33	98.57	81.95	73.70	88.33	
HG	HGNN	84.92	56.55	98.33	77.44	66.62	88.33	81.85	64.17	91.72	77.95	69.50	80.40
	WHGCN	83.36	78.57	87.20	82.88	74.90	76.90	82.69	70.83	91.43	81.13	76.36	94.54
	TriCL	86.89	86.67	83.65	85.16	80.54	78.34	83.78	85.17	81.43	83.30	79.87	81.56
	MHSA	80.53	61.50	91.42	76.46	68.06	86.55	76.15	54.33	91.42	72.88	60.79	81.39
	UH-FRL	88.48	70.23	98.00	84.12	79.50	98.00	85.38	68.75	97.64	83.19	66.79	65.50
FHG	HGNN†	88.48	69.17	96.25	82.70	73.90	83.50	84.35	76.58	86.90	81.74	76.63	79.89
	WHGCN†	86.74	86.07	84.57	85.32	81.60	83.17	84.36	67.00	95.71	81.36	76.20	96.25
	TriCL†	92.27	90.83	92.25	91.54	87.75	85.17	88.53	84.37	92.38	88.37	85.58	91.19
	MHSA†	83.93	65.50	94.29	79.90	73.90	91.67	78.84	67.33	87.14	77.23	70.41	83.91
	UH-FRL	96.36	94.40	98.75	96.58	95.45	97.50	94.29	95.00	94.23	94.61	93.78	93.81

† Indicates that the baseline method incorporates the proposed URC module and the bold font indicates the best performance term.

Table 3

The classification results of the UH-FRL method and comparison method (%) on PPMI and PSCI datasets.

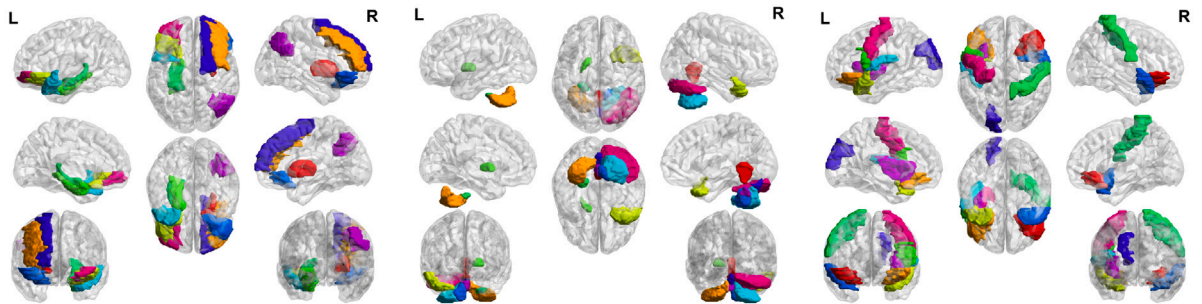
Method	NC vs. PD						NC vs. SD						
	ACC	SEN	SPE	AUC	F1	PRE	Acc	SEN	SPE	Auc	F1	PRE	
G	GCNII	56.65	59.56	68.00	79.86	48.10	51.19	81.00	73.50	82.83	78.17	78.12	78.33
	CAGNN	72.09	80.83	65.00	93.39	82.29	64.81	85.50	85.00	86.67	85.83	83.83	86.60
	BGAN	63.62	72.53	48.00	60.27	71.29	80.99	72.19	61.80	88.96	95.9	88.96	85.19
	XG_GNN	80.99	86.33	65.00	75.67	85.86	89.76	82.00	60.83	82.50	71.67	52.74	54.33
	GCNH	75.66	95.78	35.00	65.39	68.94	65.40	83.50	80.00	85.00	82.5	82.57	88.33
	HGNN	75.00	88.89	36.67	62.78	77.17	68.93	81.50	65.00	80.00	72.50	61.67	62.00
	WHGCN	81.70	89.11	58.50	73.81	84.50	84.53	83.50	70.00	73.33	71.67	62.39	57.33
	TriCL	76.45	95.50	43.50	69.50	83.77	75.66	87.50	86.67	83.33	85.00	81.56	79.67
	MHSA	78.74	86.67	63.50	75.08	84.24	83.35	79.00	70.00	86.67	78.33	65.67	65.00
	HDFIS	77.11	83.15	61.54	72.35	78.10	77.46	80.10	72.00	80.00	71.27	62.09	70.06
UH-FRL	83.90	94.00	58.58	76.29	87.21	82.55	94.00	100	87.50	93.75	94.17	91.00	
HG	HGNN	85.22	97.63	54.25	79.94	90.31	84.95	84.00	63.33	86.67	75.00	66.22	74.67
	WHGCN	86.76	96.90	82.89	89.90	80.08	71.53	89.50	79.17	95.00	87.08	81.81	87.50
	TriCL	80.16	88.60	55.64	72.12	85.00	81.91	93.50	100	90.83	95.41	91.33	86.67
	MHSA	84.61	91.22	71.00	81.11	88.74	87.74	79.00	95.00	66.67	80.83	81.33	76.67
	UH-FRL	88.96	98.88	70.33	84.61	92.05	86.68	96.00	90.00	100	95.00	90.00	90.00
FHG	HGNN†	88.24	94.55	71.16	82.86	91.14	89.21	90.00	75.83	100	87.91	81.24	90.00
	WHGCN†	88.29	87.10	89.17	88.13	91.00	96.69	95.50	86.67	100	93.33	88.00	90.00
	TriCL†	89.38	94.93	80.47	87.70	92.01	90.69	96.00	90.00	97.50	93.75	86.67	85.00
	MHSA†	88.35	97.78	70.00	83.89	92.07	87.78	85.00	75.00	91.67	83.33	79.33	93.33
	UH-FRL	94.95	95.56	91.25	93.40	95.25	95.33	100	100	100	100	100	100

- **w/o FN** removes the fuzzy layer that encodes fuzzy representations of node features in the fuzzy hypergraph encoder.
- **w/o FHE** replaces the Fuzzy Hypergraph Encoder with the ordinary hypergraph encoder to complete information aggregation of high-order structure.

Initially, we removed the URC module, and the w/o U results indicated a significant performance decline compared to configurations retaining it. This decline is primarily caused by the model's inability to deal with uncertainties in functional connectivity, which hinders accurate modeling of high-order interactions between ROIs and highlights the importance of fuzzy information in accurately modeling the synergistic interactions. Then, the result of eliminating the Fuzzy Hypergraph Convolution

Table 4
The validity evaluation of the different components for the proposed UH-FRL (%).

Method	NC vs. AD						NC vs. MCI					
	ACC	SPE	SEN	AUC	F1	PRE	ACC	SPE	SEN	AUC	F1	PRE
w/o FE	84.02	69.40	92.32	80.86	75.88	92.50	88.33	74.83	98.33	86.58	79.96	88.33
w/o FN	81.43	57.38	93.75	75.56	64.80	81.50	88.52	81.25	94.36	87.80	85.36	91.30
w/o FHE	82.12	57.74	93.57	75.65	64.14	82.07	85.19	74.92	92.08	83.50	77.28	84.33
w/o U	88.48	70.23	98.00	84.12	79.50	98.00	85.38	68.75	97.64	83.19	66.79	65.50
UH-FRL	96.36	94.40	98.75	96.58	95.45	97.50	94.29	95.00	94.23	94.61	93.78	93.81
Method	NC vs. PD						NC vs. SD					
	ACC	SPE	SEN	AUC	F1	PRE	ACC	SPE	SEN	AUC	F1	PRE
w/o FE	88.35	98.88	69.33	84.11	91.49	85.85	90.00	81.67	93.33	87.50	80.66	83.33
w/o FN	87.47	97.98	66.33	82.16	91.19	86.01	86.00	66.67	100	83.33	71.33	80.00
w/o FHE	81.70	99.09	48.33	73.71	87.94	80.47	85.50	70.00	90.00	80.00	67.50	66.00
w/o U	88.96	98.88	70.33	84.61	92.05	86.68	96.00	90.00	100	95.00	90.00	90.00
UH-FRL	94.95	95.56	91.25	93.40	95.25	95.33	100	100	100	100	100	100



(a) Location of Alzheimer's disease lesions (b) Location of Parkinson's disease lesions (c) Location of Stroke's disease lesion

Fig. 6. The visualization of the top 10 most discriminative ROIs across three datasets, obtained by computing region-wise importance scores based on the feature extraction method of study [13] for the final classification decision.

module (w/o FHC) demonstrated that neglecting fuzzy information during hyperedge aggregation leads to degraded performance. Similarly, removing the Fuzzy Layer (w/o FL) resulted in decreased performance because critical fuzzy information in node features cannot be handled, limiting the encoder's ability to capture abnormal changes in functional brain networks. Finally, substituting the proposed FHE with a standard hypergraph encoder (w/o FHE) leads to the poorest performance, as conventional hypergraph encoders are inadequate in effectively capturing fuzzy information in functional networks. These findings collectively highlight the crucial role of extracting fuzzy information from both hyperedges and node features in improving model efficacy.

5.4. Parameter sensitivity analysis

In this section, we evaluate the impact of key hyperparameters on model performance. The ξ is a tuning variable that controls the critical distance of clustering centers, with the "existence" state set to $\xi = D/\gamma$, where D is the Euclidean distance between cluster centers. And the "inexistence" state set to $\xi = 2D/\gamma$. The parameter k represents the number of fuzzy sets in the fuzzy layer. As shown in Fig. 9, smaller values of γ and k diminish the model's capacity to capture functional connectivity and ROIs features uncertainty, thereby weakening the representations of brain network fuzziness. Conversely, excessively large γ and k values lead to over-fuzzification of functional connections and ROIs features, making it more confusing to capture the uncertainty.

5.5. The time complexity analysis

We analyzed the time complexity of the UH-FRL model. For a dataset containing N subjects and M ROIs with T time points, the URC module first generates $M(M-1)/2$ relationship features by the calculation of multiple similarity metrics between ROIs, resulting in a time complexity of $O(NM^2T)$. The complexity of inferring membership degrees of connectivity states is $O(NM^2d_r)$; since $T \gg d_r$, the dominant cost in URC remains $O(NM^2T)$. In the FHE module, the L -layer Fuzzy Hypergraph Convolution aggregates multi-ROI interactions with a complexity of $O(NLMd_r)$, while the Fuzzy Layer evaluates k Gaussian membership functions for node feature fuzzification, leading to a cost of $O(NMdk)$. Hence, the total complexity of the FHE is $O(NMd(L+k))$. The Fuzzy Contrastive Strategy computes node-level and group-level contrastive losses, each involving pairwise similarity computations with complexity $O(NM^2d_r)$. In summary, the overall computational burden of UH-FRL is dominated by $O(NM^2(T+d_r))$, indicating the model's scalability for neurodegenerative disease detection. The runtime and memory usage are reported in Table 7.

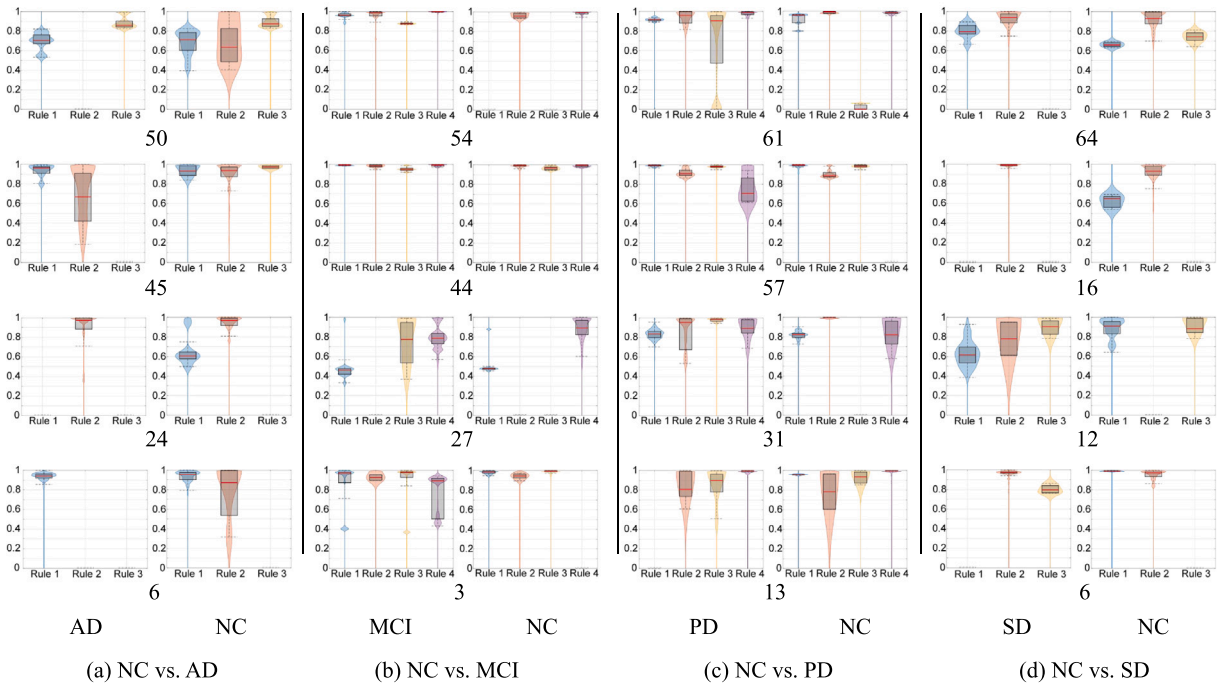


Fig. 7. The visualization of the distributional differences of the ROIs within the fuzzy rules by maximum activation degree across all disease groups (AD, MCI, PD, SD) and the NC.

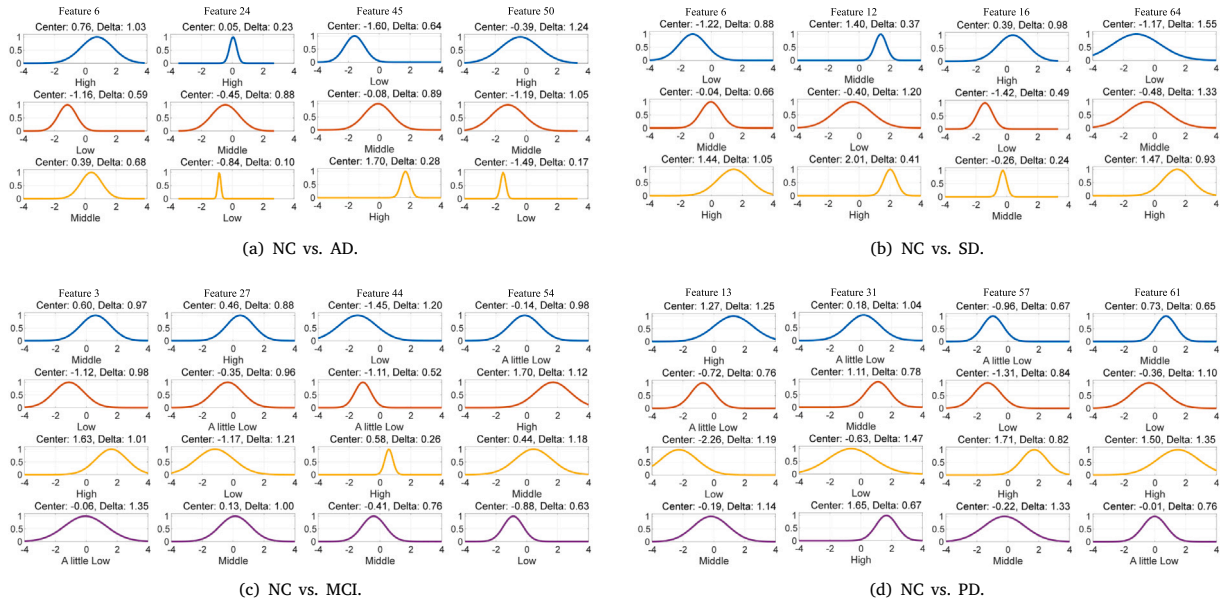


Fig. 8. The visualization of Gaussian membership functions for ROI features across different fuzzy sets in each classification task. Four feature dimensions were sampled, and the multiple Gaussian membership functions learned for each feature in its corresponding fuzzy layer were plotted.

5.6. Uncertainty analysis

Uncertainty Functional Connectivity Analysis. The construction of hypergraphs based on fuzzy theory captures the progressive degradation of functional connectivity during neurodegenerative disease progress by explicitly quantifying inherent uncertainty. To

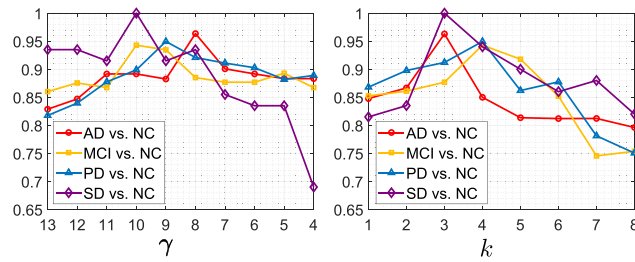


Fig. 9. Evaluation of the impact of key hyperparameters, including the number of fuzzy sets k and the critical distance $\xi = D/\gamma$ and D is the Euclidean distance between cluster centers, on the classification performance of the UH-FRL model.

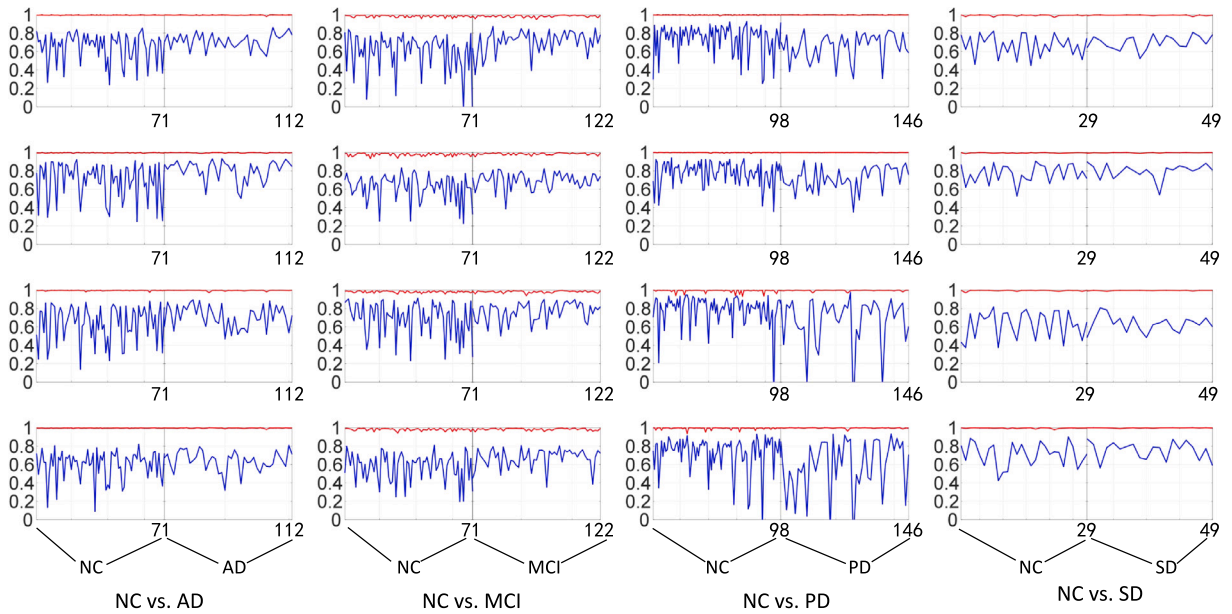


Fig. 10. Effectiveness verification of the proposed FHE encoder by randomly selecting 4 ROIs and calculating the PCC values of the features before and after encoding with the standard features through visualization. The blue curves represent the PCC values between standard features and features after FHE encoding, and the red curves represent the PCC values between standard features and features before FHE encoding.

validate this approach, we visualized functional connectivity for brain network of NC and AD subjects, comparing it with graphs and hypergraphs, as shown in Fig. 11. We observe the following: (1) The fuzzy hypergraph brain network retains crucial connections of intermediate state that highlight structural differences between AD and NC brain networks. These connections are often overlooked in conventional graph or hypergraph. (2) In contrast to the graph and hypergraph, the fuzzy hypergraph reveals a clear reduction of connections in AD subjects. This reduction is primarily caused by neuronal loss and brain atrophy, particularly in regions associated with memory, executive, and cognition function, resulting in progressive degradation of functional connectivity. These findings are consistent with previous studies [63], supporting the biological relevance of the proposed fuzzy hypergraph brain network.

Uncertainty in Node Feature. To assess the effectiveness of fuzzy information extraction from ROIs, we sampled four feature dimensions across all classification tasks and visualized their Gaussian membership functions, as shown in Fig. 8. Further, we examined the distribution of the maximum rule activation degree for subjects with disease and NC labels using the corresponding Gaussian membership functions, as illustrated in Fig. 7. The results reveal substantial differences in activation degree distributions across labels. For instance, in the AD vs. NC task, the maximum rule activation of feature 50 for AD samples is predominantly clustered in Rule 1 and Rule 3, whereas for NC subjects, it is primarily concentrated in Rule 2. These distinct patterns demonstrate that the fuzzy information extracted at ROIs captures subtle but discriminative abnormal variations, thereby enhancing the model's ability to learn discriminative representations.

Moreover, we evaluated the effectiveness of the weighted aggregation mechanism defined in Eq. (11) by comparing it with the maximum, minimum, and average operators for rule integration. As presented in Table 5, our proposed method achieved the best performance. This superiority stems from the mechanism's enhanced capacity for fine-grained characterization of fuzzy information. Notably, the maximum and minimum operators rely on extreme membership values, ignoring the rich uncertainty information

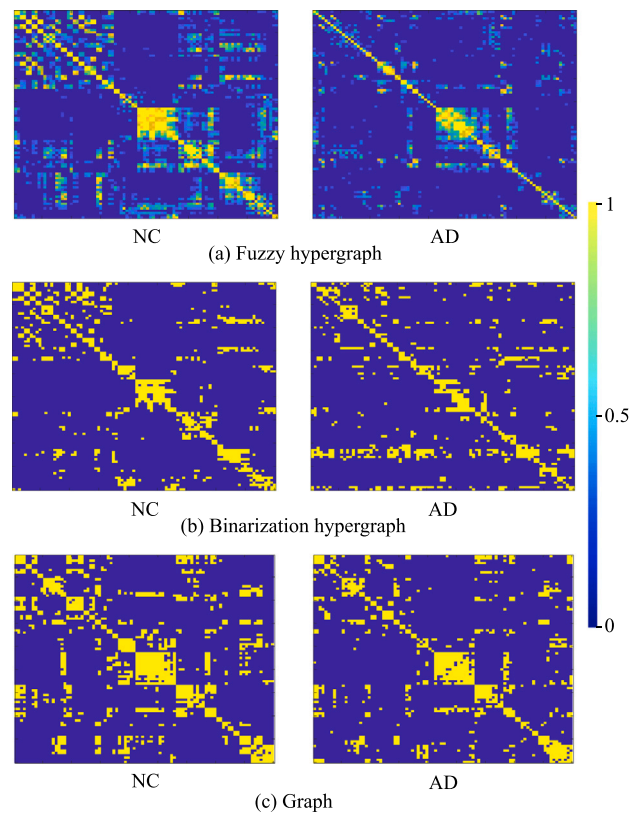


Fig. 11. The visualization and comparison of functional connectivity patterns obtained from fuzzy hypergraphs, binarization hypergraph, and graph for NC vs. AD classification task.

provided by other rules. The average operator considers all rules but over-smooths their contributions, thereby attenuating critical discriminatory features. In contrast, our learnable weighting dynamically evaluates and combines the outputs of all rules, adaptively amplifying the impact of pivotal rules and producing a more comprehensive and robust representation of feature uncertainty.

5.7. Effectiveness of Fuzzy contrastive strategy

To evaluate the effectiveness of the fuzzy contrastive strategy in capturing disease-relevant feature patterns, we investigated the impact of the strategy from the perspective of node features. First, for each category, the ROI features of samples before FHE encoding were summed and averaged to derive the standard features of the corresponding ROIs. Similarly, the standard ROI features after FHE encoding were calculated. Subsequently, we computed the Pearson Correlation Coefficient (PCC) between each ROI feature and its corresponding standard feature.

Four sampled ROIs are visualized in Fig. 10. The results demonstrate that after FHE encoding, the PCC values of ROI features substantially increased for within-class samples. This improvement indicates enhanced intra-class feature consistency and validates that the fuzzy contrastive strategy strengthens the discriminative power of feature representations without disrupting the biological significant connection structures in the brain network. Consequently, the model learns more robust representations, yielding clearer functional connectivity patterns associated with disease and ultimately improving downstream detection performance.

5.8. Most discriminative brain regions

To uncover potential biomarkers for neurodegenerative diseases, we employed the feature extraction method [13] to compute ROI importance scores, which measure each ROI's contribution to the final classification by using classifier parameters of the UH-FRL model. The top 10 ROIs with the highest scores are listed in Table 6 and visualized in Fig. 6 to illustrate their potential biological significance. For the Alzheimer's disease, the most discriminative ROIs include the PHG.L, which serves as a hub for encoding, retrieval, and contextual integration. The HIP.L is crucial for new memory formation and spatial learning, while the SFGdor.R is involved in higher-order cognitive control and working memory. These findings consistent with previous studies on AD-related functional alterations [64]. For the Parkinson's disease, the top-ranked ROIs were predominantly located in the cerebellum, consistent with prior research [65]. Specifically, the PAL.L is associated with the indirect pathway regulating movement, the Cere8.R

Table 5

Performance comparison of max, min and the proposed aggregation operators method of fuzzy rules in the fuzzy layer (%).

Method	NC vs. AD						NC vs. MCI					
	ACC	SPE	SEN	AUC	F1	PRE	ACC	SPE	SEN	AUC	F1	PRE
Max	90.15	74.88	100	87.44	84.26	100	87.69	80.99	93.03	87.01	82.83	91.80
Min	81.43	57.38	93.75	75.56	64.80	81.50	84.42	73.67	93.15	83.41	78.04	92.91
Mean	85.15	63.80	98.57	81.19	72.31	98.00	86.92	80.25	90.99	85.62	81.70	90.23
UH-FRL	96.36	94.40	98.75	96.58	95.45	97.50	94.29	95.00	94.23	94.61	93.78	93.81
Method	NC vs. PD						NC vs. SD					
	ACC	SPE	SEN	AUC	F1	PRE	ACC	SPE	SEN	AUC	F1	PRE
Max	91.31	97.97	80.83	89.40	93.36	90.27	93.49	95.00	87.50	91.25	91.90	92.50
Min	86.92	98.75	64.41	81.58	90.65	84.96	89.49	86.67	86.67	84.17	83.14	81.67
Mean	89.06	95.00	79.17	87.08	91.36	88.76	91.50	100	81.67	90.83	91.57	87.50
UH-FRL	94.95	95.56	91.25	93.40	95.25	95.33	100	100	100	100	100	100

Table 6

The detailed information on the top 10 ROIs that are most discriminative for the final classification, and the corresponding importance scores.

Alzheimer's disease			Parkinson's disease			Stroke's disease		
AAL ID	Region	Score	AAL ID	Region	Score	AAL ID	Region	Score
74	PUT.R	0.23822	111	Verm4_5	0.45891	16	ORBinf.R	0.18871
8	MFG.R	0.21602	103	Cere8.L	0.41700	15	ORBinf.L	0.07676
15	ORBinf.L	0.20260	88	TPOmid.R	0.36181	83	TPOsup.L	0.07142
39	PHG.L	0.19996	75	PAL.L	0.31839	11	IFGoperc.L	0.06821
37	HIP.L	0.19765	107	Cere10.L	0.30412	58	PoCG.R	0.06233
83	TPOsup.L	0.19435	104	Cere8.R	0.25100	17	ROL.L	0.05575
16	ORBinf.R	0.19306	106	Cere9.R	0.24029	84	TPOsup.R	0.04093
4	SFGdor.R	0.18498	113	Verm7	0.23938	49	SOG.L	0.03868
66	ANG.R	0.18137	115	Verm9	0.20856	29	INS.L	0.03712
9	ORBmid.L	0.17443	92	CC1.R	0.20263	1	PreCG.L	0.03711

Table 7

Time and storage consumption of different methods.

Method	Running time (s)				Memory usage (MB)			
	NC vs. AD	NC vs. MCI	NC vs. PD	NC vs. SD	NC vs. AD	NC vs. MCI	NC vs. PD	NC vs. SD
BGAN	4650.98	2339.49	5001.64	922.45	123.56	123.56	148.00	78.28
WHGCN	491.81	491.96	521.62	539.88	106.89	106.89	148.07	78.28
TriCL	1028.44	936.85	1075.65	447.85	123.54	106.80	148.00	78.26
UH-FRL	222.11	225.69	424.14	314.64	103.08	106.09	148.00	78.31

is involved in motor coordination and fine motor control, while the Cere10.L is associated with balance regulation, vestibular processing, and autonomic aspects of motor control. For the Stroke's disease, vital ROIs include the PreCG.L, which acts as the primary motor cortex controlling voluntary movements of the contralateral body. The INS.L combines interoceptive, gustatory, and pain signals. The IFGoperc.L is a core node of the language network for speech production and motor planning. These identified ROIs are critical for understanding stroke lesions and align with findings from [66].

6. Conclusion

This paper investigates the uncertainty within functional brain networks and introduces a novel brain disease detection UH-FRL approach by applying fuzzy theory to address this challenge. The key idea lies in utilizing multi-similarity measurement methods to construct relationship features, followed by integrating fuzzy theory to infer the functional connectivity states to quantify the uncertainty. Comprehensive experiments in two public and a private datasets indicate that UH-FRL achieves state-of-the-art performance, demonstrating significant improvements in detection accuracy over existing approaches. Our work introduces a new uncertainty-modeling paradigm for neuroimaging-based detection and pioneers a promising avenue for integrating fuzzy theory with hypergraph learning in biomedical network analysis.

CRedit authorship contribution statement

Manman Yuan: Writing – review & editing, Supervision, Resources, Funding acquisition, Conceptualization. **Can Yin:** Writing – original draft, Software, Methodology, Conceptualization. **Junlin Li:** Visualization, Supervision, Investigation. **Jun Hu:** Validation, Resources. **Huijia Li:** Visualization, Resources, Investigation, Formal analysis. **Matjaž Perc:** Validation, Supervision, Investigation, Funding acquisition.

Declaration of competing interest

The authors declare that they have no known competing financial interests or personal relationships that could have appeared to influence the work reported in this paper.

Acknowledgments

This research was supported by the Slovenian Research and Innovation Agency (Grant No. P1-0403), and the National Natural Science Foundation of China (Grant No. 62466042, Grant No. 72571150).

Data availability

We have used two public datasets, which are publicly available at: <https://adni.loni.usc.edu> and <https://www.ppmi-info.org>.

References

- [1] Vigo D, Thornicroft G, Atun R. Estimating the true global burden of mental illness. *Lancet Psychiatry* 2016;3(2):171–8.
- [2] Zhang Z, Yang X. Research on coupled dynamic modeling of the related potassium buffering function in astrocytes under Alzheimer's disease environment. *Chaos Solitons Fractals* 2025;193:116111.
- [3] Mukhtar R, Chang C-Y, Mukhtar A, Raja MJAA, Chaudhary NI, Khan ZA, Raja MAZ. A novel fractional Parkinson's disease onset model involving α -syn neuronal transportation and aggregation: A treatise on machine predictive networks. *Chaos Solitons Fractals* 2025;194:116269.
- [4] Joaquin M, D P-ES, Hernan H, Raul G-G, Agustina L, Sol F, de Paula França RE, Claudia D-A, Alberto A-FJ, I BM, et al. Social exposome and brain health outcomes of dementia across Latin America. *Nat Commun* 2025;16(1):8196.
- [5] Papakostas G. Managing partial response or nonresponse: Switching, augmentation, and combination strategies for major depressive disorder. *J Clin Psychiatry* 2009;70 Suppl 6:16–25.
- [6] Yuan M, Li Y, Zheng M. Novel intermittent pinning control beyond the semigroup framework for fractional-order delayed inertial memristive neural networks. *Chaos Solitons Fractals* 2026;202:117568.
- [7] Ma J, Luo C, Hou J, Zhao K. Self-promoted clustering-based contrastive learning for brain networks pretraining. In: International joint conference on artificial intelligence – IJCAI. 2024, p. 1164–72.
- [8] Yu S, Jin S, Li M, Sarwar T, Xia F. Long-range brain graph transformer. In: Advances in neural information processing systems – NeurIPS. Vol. 37, 2024, p. 24472–95.
- [9] Zeng Y, Lin J, Li Z, Xiao Z, Wang C, Ge X, Wang C, Huang G, Liu M. Adaptive node feature extraction in graph-based neural networks for brain diseases diagnosis using self-supervised learning. *NeuroImage* 2024;297:120750.
- [10] Mou SF, Abdur Razzak SM. Brain disease classification from MRI scans using EfficientNetB0 feature extraction. In: International Conference on Information and Communication Technology for Sustainable Development – ICICT4SD. 2023, p. 336–40.
- [11] Liu M, Zhang H, Liu M, Chen D, Zhuang Z, Wang X, Zhang L, Peng D, Wang Q. Randomizing human brain function representation for brain disease diagnosis. *IEEE Trans Med Imaging* 2024;43(7):2537–46.
- [12] Liu J, Cui W, Chen Y, Ma Y, Dong Q, Cai R, Li Y, Hu B. Deep fusion of multi-template using spatio-temporal weighted multi-hypergraph convolutional networks for brain disease analysis. *IEEE Trans Med Imaging* 2024;43(2):860–73.
- [13] Bi X-A, Huang Y, Shen W, Yang Z, Mao Y, Xu L, Liu Z. Brain-inspired fuzzy graph convolution network for Alzheimer's disease diagnosis based on imaging genetics data. *IEEE Trans Fuzzy Syst* 2025;33(6):1698–712.
- [14] Yuan M, Li J, Li Y, Xiong W, Chen G. Designing pinning control synchronization scheme for inertial memristive neural networks with dynamic granger causality. *IEEE Trans Autom Sci Eng* 2025;22:20934–50.
- [15] Zuo Q, Wu H, Chen CLP, Lei B, Wang S. Prior-guided adversarial learning with hypergraph for predicting abnormal connections in Alzheimer's disease. *IEEE Trans Cybern* 2024;54(6):3652–65.
- [16] Li Z, Han B, Wang D, Yan J, Zhang X, Yin L. Hypergraph-based brain network switching rate and its application in epilepsy. *Chaos Solitons Fractals* 2026;203:117653.
- [17] Hao X, Li J, Ma M, Qin J, Zhang D, Liu F. Hypergraph convolutional network for longitudinal data analysis in Alzheimer's disease. *Comput Biol Med* 2024;168:107765.
- [18] Feng Y, You H, Zhang Z, Ji R, Gao Y. Hypergraph neural networks. In: The AAAI Conference On Artificial Intelligence – AAAI. 33, (01):2019, p. 3558–65.
- [19] Luo Y, Chen H, Yin T, Horng S-J, Li T. Dual hypergraphs with feature weighted and latent space learning for the diagnosis of Alzheimer's disease. *Inf Fusion* 2024;112:102546.
- [20] Liu M, Gao Y, Yap P-T, Shen D. Multi-hypergraph learning for incomplete multimodality data. *IEEE J Biomed Health Inform* 2018;22(4):1197–208.
- [21] Kudela M, Harezlak J, Lindquist MA. Assessing uncertainty in dynamic functional connectivity. *NeuroImage* 2017;149:165–77.
- [22] Li Y, Yang B, Pan D, Zeng A, Wu L, Yang Y. Early diagnosis of Alzheimer's disease based on multimodal hypergraph attention network. In: IEEE international conference on multimedia and expo – ICME. 2023, p. 192–7.
- [23] Aviles-Rivero AI, Runkel C, Papadakis N, Kourtzi Z, Schönlieb C-B. Multi-modal hypergraph diffusion network with dual prior for Alzheimer classification. In: Medical image computing and computer assisted intervention – MICCAI. 2022, p. 717–27.
- [24] Cao P, Wen G, Yang W, Liu X, Yang J, Zaiane O. A unified framework of graph structure learning, graph generation and classification for brain network analysis. *Appl Intell* 2022;53(6):6978–91.
- [25] Cui H, Dai W, Zhu Y, Kan X, Gu AAC, Lukemire J, Zhan L, He L, Guo Y, Yang C. BrainGB: A benchmark for brain network analysis with graph neural networks. *IEEE Trans Med Imaging* 2023;42(2):493–506.
- [26] Teng M, Wang Y, Gao C, Dmitrichev AS, Kasatkin DV, Maslennikov OV, Nekorkin VI. Similarity-smooth graph contrastive learning for community detection in adaptive oscillatory networks. *Chaos Solitons Fractals* 2025;200:116937.
- [27] Chen L, Liang W. Disentangling multi-factor effects via graph contrastive learning for travel recommendation. *Appl Soft Comput* 2026;186:114095.
- [28] Li X, He Y, Li J, Zhu K, Chang J, Yu J. Multi-representation space recommendation with graph contrastive learning. *Expert Syst Appl* 2026;297:129274.
- [29] Song Y, Gu Y, Li T, Qi J, Liu Z, Jensen CS, Yu G. CHGNN: A semi-supervised contrastive hypergraph learning network. *IEEE Trans Knowl Data Eng* 2024;36(9):4515–30.
- [30] Song X, Wu K, Chai L. Brain network analysis of schizophrenia patients based on hypergraph signal processing. *IEEE Trans Image Process* 2023;32:4964–76.
- [31] Wang Y, Gao S. Evolution of cooperation on hypergraphs with heterogeneous update dynamics. *Chaos Solitons Fractals* 2026;204:117776.

- [32] Han X, Xue R, Feng J, Feng Y, Du S, Shi J, Gao Y. Hypergraph foundation model for brain disease diagnosis. *IEEE Trans Neural Netw Learn Syst* 2025;36(10):17702–16.
- [33] Han X, Lei M, Li J. Hypergraph-based semantic and topological self-supervised learning for brain disease diagnosis. *Pattern Recognit* 2026;169:111921.
- [34] Li W, Jie B, Wu Z, Zhou J. Hypergraph attention-based feature extraction method for the classification of brain diseases. In: *International conference on computer vision, image and deep learning – CVIDL*. 2024, p. 646–50.
- [35] Wang X, Xin J, Wang Z, Qu L, Li J, Wang Z. Graph kernel of brain networks considering functional similarity measures. *Comput Biol Med* 2024;171:108148.
- [36] Xiao L, Wang J, Kassani PH, Zhang Y, Bai Y, Stephen JM, Wilson TW, Calhoun VD, Wang Y-P. Multi-hypergraph learning-based brain functional connectivity analysis in fMRI data. *IEEE Trans Med Imaging* 2020;39(5):1746–58.
- [37] Wang W, Xiao L, Qu G, Calhoun VD, Wang Y-P, Sun X. Multiview hyperedge-aware hypergraph embedding learning for multisite, multiatlas fMRI based functional connectivity network analysis. *Med Image Anal* 2024;94:103144.
- [38] Cai H, Zhou Z, Yang D, Wu G, Chen J. Discovering brain network dysfunction in Alzheimer's disease using brain hypergraph neural network. In: *Medical image computing and computer assisted intervention – MICCAI*. 2023, p. 230–40.
- [39] Bi X-A, Wang Y, Luo S, Chen K, Xing Z, Xu L. Hypergraph structural information aggregation generative adversarial networks for diagnosis and pathogenetic factors identification of Alzheimer's disease with imaging genetic data. *IEEE Trans Neural Netw Learn Syst* 2024;35(6):7420–34.
- [40] Munir K, de Ramón-Fernández A, Iqbal S, Javaid N. Neuroscience patient identification using big data and fuzzy logic—An Alzheimer's disease case study. *Expert Syst Appl* 2019;136:410–25.
- [41] Sharma R, Goel T, Tanveer M, Dwivedi S, Murugan R. FAF-DRVFL: Fuzzy activation function based deep random vector functional links network for early diagnosis of Alzheimer disease. *Appl Soft Comput* 2021;106:107371.
- [42] Horng Y-J, Chen S-M, Chang Y-C, Lee C-H. A new method for fuzzy information retrieval based on fuzzy hierarchical clustering and fuzzy inference techniques. *IEEE Trans Fuzzy Syst* 2005;13(2):216–28.
- [43] Yu J, Hipel KW, Kilgour DM, Fang L, Yin K. Graph model under unknown and fuzzy preferences. *IEEE Trans Fuzzy Syst* 2020;28(2):308–20.
- [44] Zhang X, Ma Z. Fuzzy RDF knowledge graph embeddings through vector space model. *IEEE Trans Fuzzy Syst* 2023;31(3):835–44.
- [45] Zhang C-Y, Lin Y-N, Chen CLP, Yao H-Y, Cai H-C, Fang W-P. Fuzzy representation learning on graph. *IEEE Trans Fuzzy Syst* 2023;31(10):3358–70.
- [46] Lin Y-N, Cai H-C, Zhang C-Y, Yao H-Y, Philip Chen CL. Fuzzy neural network for representation learning on uncertain graphs. *IEEE Trans Fuzzy Syst* 2024;32(9):5259–71.
- [47] Liu H, Zhu T, Shang F, Liu Y, Lv D, Yang S. Deep fuzzy graph convolutional networks for PolSAR imagery pixelwise classification. *IEEE J Sel Top Appl Earth Obs Remote Sens* 2021;14:504–14.
- [48] Wei T, Hou J, Feng R. Fuzzy graph neural network for few-shot learning. In: *International joint conference on neural networks – IJCNN*. 2020, p. 1–8.
- [49] Tanveer M, Sajid M, Akhtar M, Quadir A, Goel T, Aimen A, Mitra S, Zhang Y-D, Lin CT, Ser JD. Fuzzy deep learning for the diagnosis of Alzheimer's disease: Approaches and challenges. *IEEE Trans Fuzzy Syst* 2024;32(10):5477–92.
- [50] Ieracitano C, Mammone N, Versaci M, Varone G, Ali A-R, Armentano A, Calabrese G, Ferrarelli A, Turano L, Tebala C, Hussain Z, Sheikh Z, Sheikh A, Sceni G, Hussain A, Morabito FC. A fuzzy-enhanced deep learning approach for early detection of Covid-19 pneumonia from portable chest X-ray images. *Neurocomputing* 2022;481:202–15.
- [51] Krleža D, Fertalj K. Graph matching using hierarchical fuzzy graph neural networks. *IEEE Trans Fuzzy Syst* 2017;25(4):892–904.
- [52] Zhou T, Li M, Ruan S, Luo T, Jiang B, Zhu J, Ma P, Yang D, Yang G. A reliable framework for brain tumor segmentation via multi-modal fusion and uncertainty modeling. *Inf Fusion* 2026;129:104085.
- [53] Chen Y, Ding W, Gao S, Yang J, Zhou T, Hua Q, Fu F. Uncertainty-aware multi-view evidence fusion for feature selection in brain network analysis. *Inf Fusion* 2026;130:104083.
- [54] Li A, Deng Z, Zhang W, Xiao Z, Choi K-S, Liu Y, Hu S, Wang S. Multiview transfer representation learning with TSK fuzzy system for EEG epilepsy detection. *IEEE Trans Fuzzy Syst* 2024;32(1):38–52.
- [55] Chen M, Wei Z, Huang Z, Ding B, Li Y. Simple and deep graph convolutional networks. In: *The 37th international conference on machine learning – ICML*. Vol. 119, 2020, p. 1725–35.
- [56] Chen J, Chen S, Gao J, Huang Z, Zhang J, Pu J. Exploiting neighbor effect: Conv-agnostic GNN framework for graphs with heterophily. *IEEE Trans Neural Netw Learn Syst* 2023.
- [57] Zhou Z, Wang Q, An X, Chen S, Sun Y, Wang G, Yan G. A novel graph neural network method for Alzheimer's disease classification. *Comput Biol Med* 2024;180:108869.
- [58] Qiu X, Wang F, Sun Y, Lian C, Ma J. Towards graph neural networks with domain-generalizable explainability for fMRI-based brain disorder diagnosis. In: *Medical image computing and computer assisted intervention – MICCAI*. Vol. LNCS 15002, 2024, p. 454–64.
- [59] Cavallo A, Grohnfeldt C, Russo M, Lovisotto G, Vassio L. GCNH: A simple method for representation learning on heterophilous graphs. In: *International joint conference on neural networks – IJCNN*. 2023, p. 1–8.
- [60] Lee D, Shin K. I'm me, we're us, and i'm us: Tri-directional contrastive learning on hypergraphs. In: *The AAAI Conference On Artificial Intelligence – AAAI*. 37, (7):2023, p. 8456–64.
- [61] Yuan M, Jia W, Luo X, Ye J, Zhu P, Li J. MHSA: A multi-scale hypergraph network for mild cognitive impairment detection via synchronous and attentive fusion. In: *International conference on bioinformatics and biomedicine – BIBM*. 2024, p. 2808–15.
- [62] Xue G, Wang J, Zhang K, Pal NR. High-dimensional fuzzy inference systems. *IEEE Trans Syst Man Cybern Syst* 2024;54(1):507–19.
- [63] Dennis EL, Thompson PM. Functional brain connectivity using fMRI in aging and Alzheimer's disease. *Neuropsychol Rev* 2014;24:49–62.
- [64] Mathys H, Boix CA, Akay LA, Xia Z, Davila-Velderrain J, Ng AP, Jiang X, Abdelhady G, Galani K, Mantero J, et al. Single-cell multiregion dissection of Alzheimer's disease. *Nature* 2024;632(8026):858–68.
- [65] Alushaj E, Kuurstra A, Menon RS, Ganjavi H, Morava A, Sharma M, Kashgari A, Barr J, Reisman W, Khan AR, et al. Midbrain and pallidal iron changes identify patients with REM sleep behaviour disorder and Parkinson's disease. *npj Parkinson's Dis* 2025;11(1):84.
- [66] Hernandez Petzsche MR, De La Rosa E, Hanning U, Wiest R, Valenzuela W, Reyes M, Meyer M, Liew S-L, Kofler F, Ezhov I, et al. ISLES 2022: A multi-center magnetic resonance imaging stroke lesion segmentation dataset. *Sci Data* 2022;9(1):762.